Photoelectrochemical performance of TiO$_2$-nanotube-array film modified by decoration of TiO$_2$ via liquid phase deposition

Yuyuan Zhang [a,b], Xinjun Li [a,*], Manzhi Feng [a], Fengling Zhou [a], Jinzhu Chen [a]

[a] Key Laboratory of Renewable Energy and Gas Hydrate, Guangzhou Institute of Energy Conversion, Chinese Academy of Sciences, Guangzhou 510640, China
[b] Graduate University of Chinese Academy of Sciences, Beijing 100049, China

ARTICLE INFO

ABSTRACT

TiO$_2$-nanotube-array film, fabricated by electrochemical anodization of Ti foil, was modified by TiO$_2$ nanoparticle decoration via a liquid phase deposition (LPD) process. The films were characterized by FESEM, XRD and UV/Vis spectroscopy. For TiO$_2$-nanotube-array films employed as photoanodes, the photoelectrochemical behaviors were investigated in a three-electrode electrochemical system under UV illumination. By integrating TiO$_2$-nanotube-array films into the DSSC structure using a commercially available ruthenium-based dye, the photoelectric conversion performances were also investigated. The results show that TiO$_2$ nanotube arrays have been decorated by TiO$_2$ nanoparticles via LPD. The improved photoelectrochemical performances for the decorated TiO$_2$-nanotube-array film could be attributed to the effective charge separation. An overall 114.5% increase of the photoelectric conversion efficiency of the DSSC has been achieved owing to LPD modification on the TiO$_2$-nanotube-array film.

1. Introduction

Dye-sensitized solar cells (DSSCs) have attracted considerable attention as a potential cost-effective alternative to conventional silicon semiconductor solar cells since 1991 [1]. In order to achieve higher photoelectric conversion efficiency, a lot of efforts have been made on nanocrystalline semiconductors, sensitized dyes, electrolytes and so on. TiO$_2$ with wide band gap (3.2 eV) is an excellent anode material for DSSCs owing to the inhibition of charge recombination to prolong the carrier lifetime [2]. Extensive research has been dedicated to studying TiO$_2$ anode with various structures, such as nanoparticle, nanotube, nanowire, nanorod and hybrid structure [3–7]. Among them, the TiO$_2$ nanotube has been promising as a material in solar energy conversion due to its special structure [8–11] and better performance for light harvesting.

Owing to their precisely controlled dimensions [12,13], TiO$_2$ nanotube arrays have attracted considerable interest in many fields. In 1999, Zwilling et al. [14,15] first proposed the anodization method of Ti foil to fabricate the TiO$_2$ porous film with columnar pores. Later in 2001, Grimes et al. fabricated highly ordered TiO$_2$ nanotube arrays by anodization. They also applied TiO$_2$ nanotube arrays on FTO glasses to DSSCs in 2006 [9]. In recent years, the modification on TiO$_2$-nanotube-array films has been paid more attentions to achieve higher efficiency

in DSSCs. For example, TiCl$_4$ solution post-treatment has been currently used as a modification method for the TiO$_2$-nanotube-array film to improve the photoelectric conversion performance of DSSCs [9,16].

Herein, we report a new modification method on the TiO$_2$-nanotube-array film by TiO$_2$ nanoparticle decoration via a liquid phase deposition (LPD) process. For the films employed as photoanodes, the photoelectrochemical behaviors under UV illumination and photoelectric conversion performances in DSSCs under stimulated sunlight were also investigated.

2. Experimental

2.1. The preparation and modification of TiO$_2$-nanotube-array films

2.1.1. Materials

All reagents are of analytical grade and used without any further purification. N-719 dye was obtained from Solaronix, Switzerland. Chloroplatinic acid hexahydrate (H$_2$PtCl$_6$·6H$_2$O, g37.5% as Pt), copper foil, lithium iodide (LiI), iodide (I$_2$) and 4-*tert*-butylpyridine were supplied by Westingarea Corporation. Ti foil (250 μm thick, 99.5% purity) was purchased from Shenzhen City Xuguang Titanium Co., LTD. Hydrofluoric acid (HF), nitrate acid (HNO$_3$), sodium sulfate (Na$_2$SO$_4$), sodium hydroxide (NaOH) and anhydrous acetonitrile were obtained from Guangzhou Chemical Reagent Factory. Ammonium hexafluorotitanate ((NH$_4$)$_2$TiF$_6$) and boric acid (H$_3$BO$_3$) were purchased from Shanghai SSS Reagent CO., LTD and Guangdong Guanghua Chemical Factory Co., LTD, respectively.
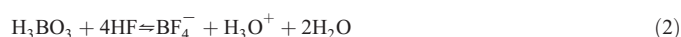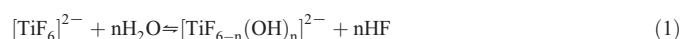
* Corresponding author. Tel.: +86 20 87057781; fax: +86 20 87057767.
E-mail address: lixj@ms.giec.ac.cn (X. Li).
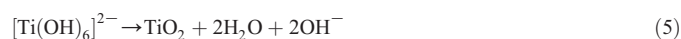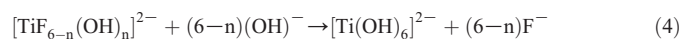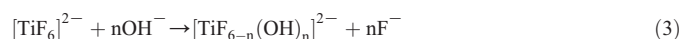
2.1.2. Preparation of TiO₂-nanotube-array films

TiO₂-nanotube-array film was prepared on Ti foil following the typical procedure [12]. Ti foil with an area of 1.5×2.5 cm^2 was subsequently pre-treated by mechanical polishing, ultrasonic degreasing and chemical polishing with a solution consisting of HF:HNO₃:H₂O = 1:4:5 (volume ratio). Then it was rinsed with deionized water and dried in nitrogen. The electrochemical anodization of Ti foil was carried out in a two-electrode cell with Ti foil as the working electrode, copper foil as the counter electrode (4 cm separation) and 1 wt.% HF aqueous solution used as electrolyte. The anodization process was operated under a constant potential of 20 V at room temperature with vigorous magnetic agitation. After 35 min of anodization, the anodized Ti foil was rinsed with deionized water thoroughly to remove the surface residue.

2.1.3. Modification of the TiO₂-nanotube-array film by liquid phase deposition

A solution for LPD was prepared by mixing pre-filtrated aqueous (NH₄)₂TiF₆ (0.1 mol/L) and H₃BO₃ (0.3 mol/L) [17]. The above fresh anodized Ti foil was immersed into the pre-treated solution for deposition. The ligand-exchange equilibrium reactions occurring on the anodized Ti foil are shown as below [18]:

$$[\text{TiF}_6]^{2-} + n\text{H}_2\text{O} \rightleftharpoons [\text{TiF}_{6-n}(\text{OH})_n]^{2-} + n\text{HF} \tag{1}$$

$$\text{H}_3\text{BO}_3 + 4\text{HF} \rightleftharpoons \text{BF}_4^- + \text{H}_3\text{O}^+ + 2\text{H}_2\text{O} \tag{2}$$

Through a hydrolysis process, $[\text{TiF}_6]^{2-}$ finally turns into TiO₂ with $[\text{TiF}_{6-n}(\text{OH})_n]^{2-}$ and $[\text{Ti(OH)}_6]^{2-}$ as the intermediate products.

$$[\text{TiF}_6]^{2-} + n\text{OH}^- \rightarrow [\text{TiF}_{6-n}(\text{OH})_n]^{2-} + n\text{F}^- \tag{3}$$

$$[\text{TiF}_{6-n}(\text{OH})_n]^{2-} + (6-n)(\text{OH})^- \rightarrow [\text{Ti(OH)}_6]^{2-} + (6-n)\text{F}^- \tag{4}$$

$$[\text{Ti(OH)}_6]^{2-} \rightarrow \text{TiO}_2 + 2\text{H}_2\text{O} + 2\text{OH}^- \tag{5}$$

After deposition for 40 min, the modified foil was thoroughly washed by deionized water in order to remove the surface residue. Then the fresh anodized foil and LPD modified foil were dried at 80 °C for 5 h and subsequently calcined at 500 °C in the air for 1 h. The calcined samples with and without modification are marked as TND and TNT, respectively.

2.2. Characterization

The morphology of TiO₂-nanotube-array films was observed by the field emission scanning electron microscopy (FESEM, LEO1530VP, Zeiss, Germany) equipped with an Energy Dispersive X-ray Detector (EDX, EDAX Incorporated, American). The acceleration voltage was 8 kV, providing a 2.5 nm point resolution.

The phase identification of TiO₂-nanotube-array films was performed by X-ray diffraction (XRD, X'Pert-PRO, PANalytical, Holland) equipped with Cu Kα radiation ($\lambda = 0.154056$ nm) at an accelerating voltage of 40 kV and a current of 40 mA. The patterns were recorded in the 2θ range from 20° to 70° at a scan rate of 1.5°/min.

The diffuse reflectance spectra (DRS) of TiO₂-nanotube-array films were recorded by a UV/Vis spectrophotometer (LAMBDA 750) equipped with an integrating sphere in the range of 200–600 nm. The width of slit was 2.0 nm and the step was 0.5 nm.

2.3. Photoelectrochemical characterization of TiO₂-nanotube-array films

2.3.1. Photoelectrochemical behaviors under UV illumination

Photoelectrochemical behavior, transient photocurrent (I_{ph}), linear sweep voltammetry (LSV) plots and electrochemical impedance spectroscopy (EIS) Nyquist plots, was performed in a three-electrode system which was made of a quartz cell linked to a CHI660A electrochemical workstation. The TiO₂-nanotube-array film, a Pt electrode, and a saturated calomel electrode served as working electrode, counter electrode and reference electrode, respectively. A 0.03 mol L^{-1} Na₂SO₄ aqueous solution was employed as a supporting electrolyte. All the photoelectrochemical tests were implemented under the illumination of a 300 W xenon lamp (with a UV high transmittance optical glass, 200–400 nm) at room temperature. LSV voltammograms were measured at a scan rate of 5 mV s^{-1} from −0.5 V to 0.5 V, and EIS Nyquist plots were collected from 10 Hz to 10^{-2} Hz.

2.3.2. Dye-sensitized solar cells assembly and measurement

TNT and TND with an active area of 0.6×0.6 cm^2 were soaked in an ethanol solution of N-719 dye for about 24 h. Then the dye-adsorbed TiO₂-nanotube-array film electrodes were assembled into sandwich-type cells with a counter electrode (platinum-deposited fluorine-doped tin oxide glass slice) by clamps. A drop of electrolyte composed of 0.1 M LiI, 0.05 M I₂ and 0.5 M 4-*tert*-butylpyridine in acetonitrile was introduced into the clamped electrodes by capillary. Dye loading measurement of the dye-adsorbed TNT and TND was conducted by desorbing the dye molecules in the NaOH ethanolic solution (10^{-4} M) [19]. The dye loading amount was determined by the absorbance of the completely desorbed dye solutions using a spectrophotometer (U-3010, HITACHI).

Photocurrent–voltage curves of DSSCs were measured by a CHI660A electrochemical workstation under the illumination of simulated sunlight with a 300 W xenon lamp (Changtuo, Beijing,
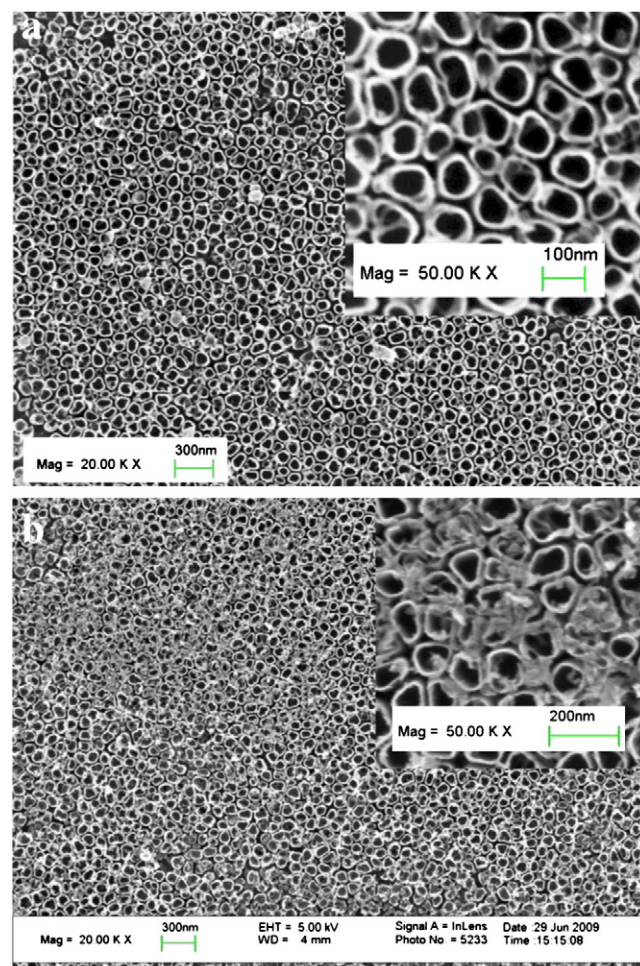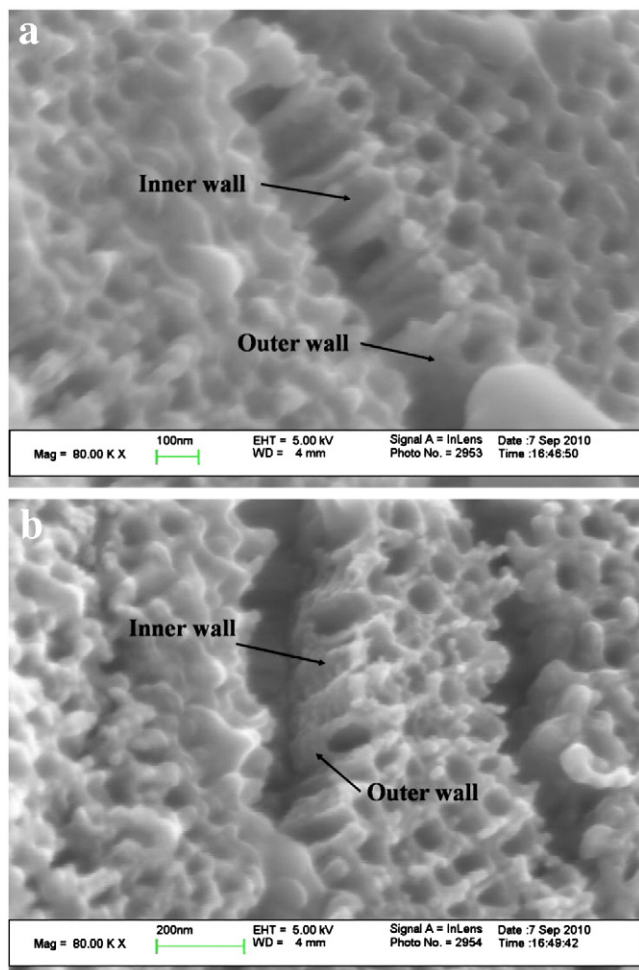

Fig. 1. FESEM images of TNT (a) and TND (b).

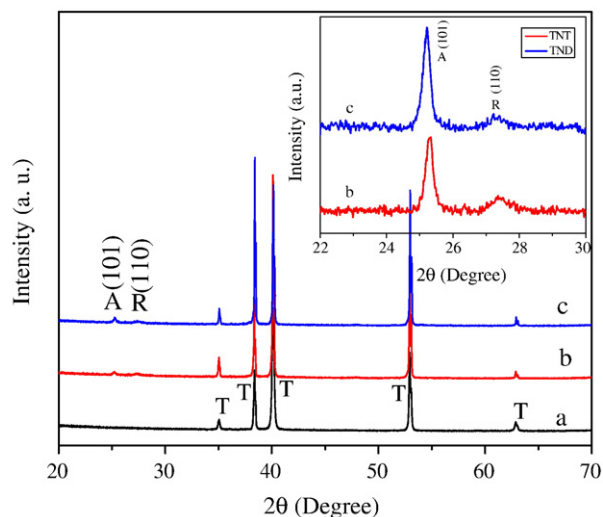**Fig. 2.** Cross-sectional FESEM images of TNT (a) and TND (b).

Fig. 3. XRD patterns of pure Ti foil (a) and the nanotube samples: TNT (b), TND (c). A, R, and T represent anatase, rutile, and titanium, respectively.

AM 1.5, 100 mW/cm^2). At the volley, open-circuit voltage decay (OCVD) experiments were conducted by monitoring the subsequent decay of open-circuit voltage (V_{oc}) in DSSCs after switching off the illumination. The potential dependent electron lifetime τ_n (really a response time) is determined by the OCVD data using the following equation [9]:

$$\tau_n = \frac{-k_B T}{e} \left(\frac{dV_{oc}}{dt} \right)^{-1} \tag{6}$$

where k_B is the Boltzmann constant, T is the absolute temperature, e is the positive elementary charge, and $^{dV_{oc}}\!/_{dt}$ is the derivative of the transient open-circuit voltage.

3. Results and discussions

3.1. Characterization of the films

Fig. 1a and b shows typical FESEM images of TNT and TND. It could be observed that the self-organized TiO$_2$ nanotubes with high aspect ratios have been fabricated on Ti foil by the electrochemical anodization technique. The diameters of these TiO$_2$ nanotubes are in the range from 30 nm to 100 nm, and the wall thickness is approximately 10 nm. The thickness of the anodized TiO$_2$-nanotube-array film is around 300 nm obtained from the profiles of FESEM figures (shown below). As shown in Fig. 1b, TiO$_2$ nanotube arrays have been decorated by TiO$_2$ nanoparticles via LPD modification. TiO$_2$ nanoparticles either engender on the tube walls or aggregate into

clusters in the tubes. However, the decoration process doesn't change the diameter or wall thickness of the nanotubes. In order to further observe the details of TiO$_2$ nanoparticle decoration in the tubes, the cross-section views were implemented and the FESEM images are shown in Fig. 2. Ascribed to TiO$_2$ nanoparticle decoration, the nanotube walls of TND become more corrugated in comparison with that of TNT. Nevertheless, the effect of LPD modification on the TiO$_2$-nanotube-array film's morphology is quite different from that of TiCl$_4$ solution modification, which could decorate TiO$_2$ nanoparticles all over the tube walls [16] and lead to the uniform increase of tube wall thickness.

Fig. 3 depicts the XRD patterns of TNT, TND and pure Ti foil. In order to differentiate the patterns of TNT and TND clearly, sectional patterns were also recorded over the 2θ range from 22° to 30° shown in the inset of Fig. 3. As shown in Fig. 3a, b and c, all characteristic peaks corresponding to pure titanium appear in all three samples. Both TNT and TND feature anatase and minor rutile phase identified by the (101) peak at 25.3° and (110) peak at 27.4°, respectively. Fig. 4 presents the DRS spectra of TNT and TND. Compared with TNT, TND exhibits a red shift of absorption edge, which can be more obvious from the differential calculation (see the inset) according to the literature [20].
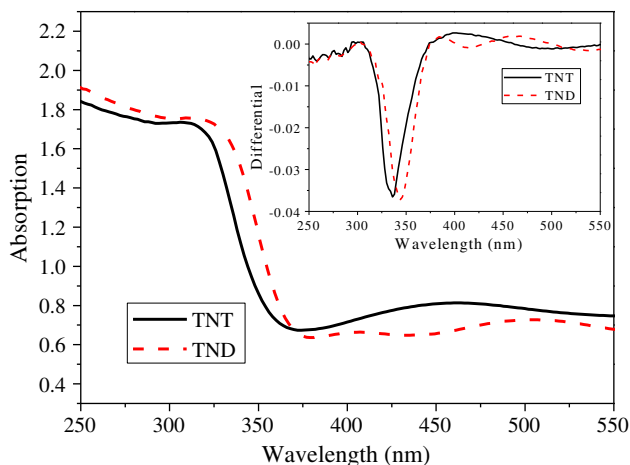

Fig. 4. Diffuse reflectance spectra of the two samples: TNT and TND. Inset: their corresponding differential curves.
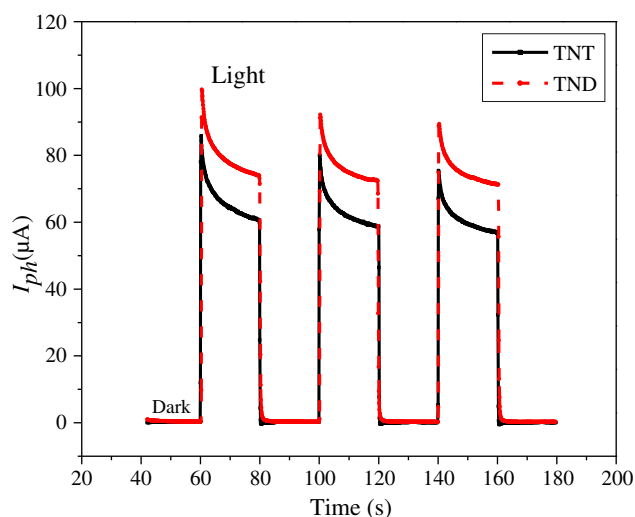
Fig. 5. Photocurrents of TiO₂-nanotube-array films under UV illumination.

3.2. Photoelectrochemical behaviors of the films under UV illumination

Electrochemical method is an effective tool to explore the photoelectrochemical properties of the TiO₂ thin film [21]. Herein, I_{ph}, LSV and EIS Nyquist were chosen to evaluate photoelectrochemical properties of the TiO₂-nanotube-array films employed as working electrodes in the three-electrode system under UV illumination.

When TiO₂ is illuminated by UV irradiation, photoelectrons are excited from the valance band to the conduction band, while positive charged photoholes remain in the valance band. I_{ph} mainly reflects the conductance value and the number of free photogenerated carriers in the semiconductor. As shown in Fig. 5, I_{ph} of TND has been augmented with LPD modification. It indicates that more free carriers could be generated in TND than that in TNT under UV illumination.

LSV is always used to investigate the behavior of minority carriers in TiO₂ [22]. Since TiO₂ is an n-type semiconductor, the minority carriers in TiO₂ are photoholes. As shown in Fig. 6, the photocurrent of TND is higher than that of TNT, which reveals that TND generates more photoholes than TNT does. When ethanol, a photohole capture agent, presents in the supporting electrolyte, the photocurrents of both samples are increased and the photocurrent increase of TND is higher than that of TNT (see Fig. 6). This further confirms that the LPD modification can facilitate generation of more photoholes in the film.
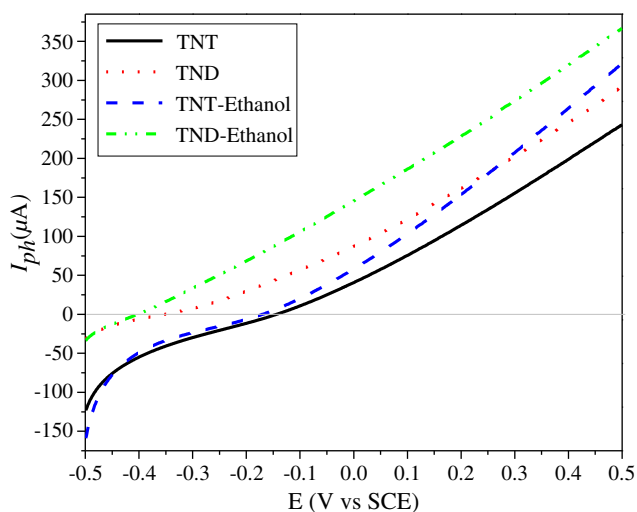

Fig. 6. LSV Plots of the TiO₂-nanotube-array films under UV illumination in 0.03 mol/L Na₂SO₄ aqueous solution with and without ethanol addition.
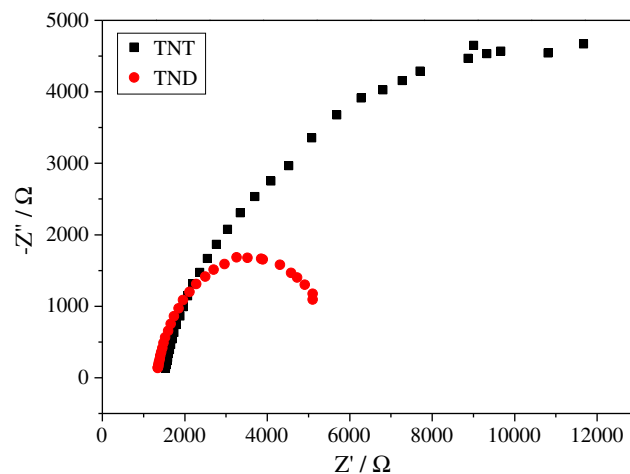

Fig. 7. EIS Nyquist plots of the TiO₂-nanotube-array films under UV illumination.

The separation efficiency of the photogenerated electron-hole pairs [23] and charge transfer resistance are always evaluated by the EIS Nyquist plots. A larger curvature radius usually represents a larger charge transfer resistance and a lower separation efficiency of the photogenerated electron-hole pairs [21]. As shown in Fig. 7, the curvature radius of TND EIS Nyquist plots is obviously smaller than that of TNT. It implies that TND possesses a relatively higher separation efficiency of the photogenerated electron-hole pairs compared with TNT does.

3.3. Performances of dye-sensitized solar cells

The photoelectric conversion performances of DSSCs with TiO₂-nanotube-array films serving as photoanodes were also investigated under the stimulated sunlight. I–V characteristics of the cells are shown in Fig. 8. The photovoltaic parameters derived from the I–V curves are listed in Table 1. The short-circuit photocurrent (I_{sc}), V_{oc}, and fill factor (FF) have been increased by 83.9%, 6.5% and 9.8%, respectively. Consequently, an overall 114.5% increase of the photoelectric efficiency (η) of the DSSC can be obtained owing to the LPD modification.

The short-circuit current density of DSSC is mainly dominated by dye loading amount and charge recombination in the TiO₂ photoanode [16,24]. The dye loading amount for TND is 1.91×10^{-8} mol/cm², which
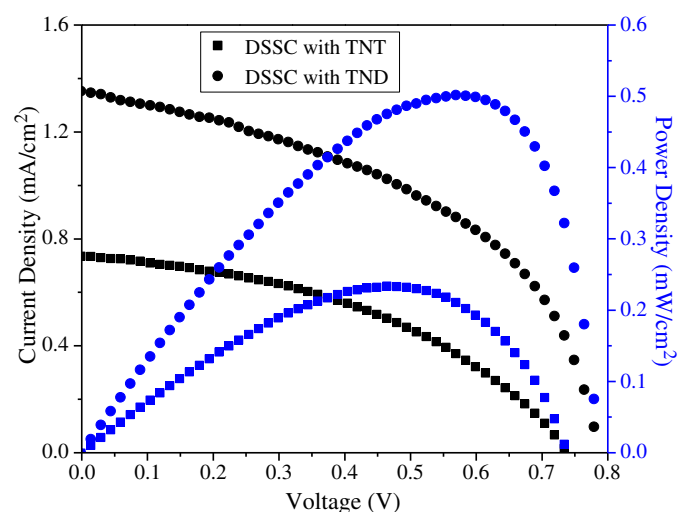

Fig. 8. I–V characteristics of the TiO₂-nanotube-array DSSCs. (AM 1.5, 100% sun illumination).

Table 1
Photovoltaic characteristics of DSSCs with TNT and TND.

Photoanodes	I_{sc} (mA/cm^2)	V_{oc} (V)	FF (%)	η (%)
TNT	0.735	0.741	42.9	0.234
TND	1.352	0.789	47.1	0.502

Fig. 10. Response time determined by open-circuit voltage decay for the TiO$_2$-nanotube-array DSSCs.

has an increase of 47% in comparison with 1.30×10^{-8} mol/cm^2 for TNT. Therefore, with respect to the overall 114.5% increase of photoelectric efficiency, the charge recombination performance in the photoanodes should be mainly related to the improvement of photoelectric conversion performances in the DSSCs.

The OCVD technique is a powerful tool to study the electron lifetime corresponding with charge separation performance in DSSCs [25]. The decay of the open-circuit voltage generally reflects the decrease of electron concentration caused by charge recombination. As shown in Fig. 9, the OCVD response of TND-based DSSC is much slower than that of TNT-based DSSC. This has also been reflected in the plot of electron lifetime (τ_n) shown in Fig. 10, which is obtained by calculation with the data in Fig. 9 according to Eq. (6). The electron lifetime of TND-based DSSC is longer than that of TNT-based DSSC at any given open-circuit voltage. Therefore, TND-based DSSC exhibits better charge separation performance caused by effective inhibition of charge recombination in the films.

3.4. Discussion

The results shown above demonstrate that the photoelectric conversion performances of DSSC with the TiO$_2$-nanotube-array film have been significantly improved by TiO$_2$ nanoparticle decoration via LPD modification. The decoration on the TiO$_2$-nanotube-array film by TiCl$_4$ post-treatment has also been testified to improve the photoconversion of DSSC [9,16,26,27], which has two important effects, dye loading and charge recombination. Our results indicate that LPD modification can result in 47% increase of dye loading and 114.5% increase of photoelectric efficiency when integrating TiO$_2$-nanotube-array films into the DSSC structure. This reveals that the charge separation performance in the photoanode should be mainly related to the improvement of photoelectric conversion performance in DSSC. This has also been confirmed in the OCVD results shown above. As mentioned in literatures [26,27], the improved photoconversion performance is ascribed to increased electron lifetime caused by TiCl$_4$ post-treatment on TiO$_2$-nanotube-array film.

Due to the lack of knowledge concerning the mechanism of TiO$_2$ nanoparticle decoration action up to now, the effect of charge separation on improved photoelectric performance of DSSC has
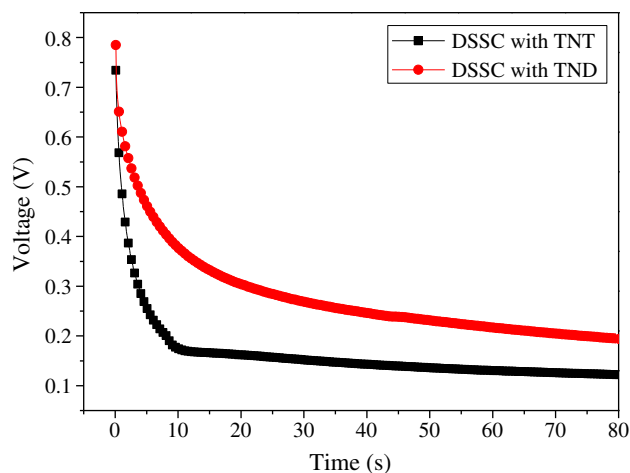
been under investigation. Mor et al. have made a hypothesis that the TiCl$_4$ treatment facilitates improved bonding between the TiO$_2$ and dye molecule, resulting in improved charge transfer [16]. Sommeling and O'Regan et al. proposed that a downward shift of the conduction band edge of TiO$_2$ gives a corresponding reduction of the charge recombination rate [26,27]. Herein we propose that the charge separation in the interior of TiO$_2$ material also has an important effect on inhibition of the charge recombination. Effective charge separation in the TiO$_2$-nanotube-array film with TiO$_2$ nanoparticle decoration has been manifested by the photoelectrochemical behaviors under UV illumination (see Figs. 5, 6, and 7). However, further investigation is necessary for clarifying the more detailed mechanism on how the LPD modified TiO$_2$-nanotube-array film act to cause charge separation.

4. Conclusion

The TiO$_2$-nanotube-array film was modified via a liquid phase deposition method to obtain TiO$_2$ nanotube array with TiO$_2$ nanoparticle decoration. The modified TiO$_2$-nanotube-array film exhibited improved photoelectrochemical performance under UV illumination. When integrating TiO$_2$-nanotube-array films into the DSSC structure, an overall 114.5% increase of photoelectric conversion efficiency has been achieved owing to the LPD modification.

Acknowledgements

Fig. 9. Open-circuit voltage decay curves of the TiO$_2$-nanotube-array DSSCs.

References

[1] B. O'Regan, M. Grätzel, Nature 353 (1991) 737.
[2] R. Jose, V. Thavasi, S. Ramakrishna, J. Am. Ceram. Soc. 92 (2009) 289.
[3] K.Y. Cheung, C.T. Yip, A.B. Djurišić, Y.H. Leung, W.K. Chan, Adv. Funct. Mater. 17 (2007) 555.
[4] K. Zhu, T.B. Vinzant, N.R. Neale, A.J. Frank, Nano Lett. 7 (2007) 3739.
[5] M. Grätzel, Nature 414 (2001) 338.
[6] M. Law, L.E. Greene, J.C. Johnson, R. Saykally, P.D. Yang, Nat. Mater. 4 (2005) 455.
[7] M. Paulose, K. Shankar, O.K. Varghese, G.K. Mor, B. Hardin, C.A. Grimes, Nanotechnology 17 (2006) 1446.
[8] M.R. Hoffmann, S.T. Martin, W. Choi, D.W. Bahnemann, Chem. Rev. 95 (1995) 69.
[9] G.K. Mor, K. Shankar, M. Paulose, O.K. Varghese, C.A. Grimes, Nano Lett. 6 (2006) 215.
[10] M. Grandcolas, A. Louvet, N. Keller, V. Keller, Angew. Chem. Int. Ed. 48 (2009) 161.

[11] K.Y. Chun, B.W. Park, Y.M. Sung, D.J. Kwak, Y.T. Hyun, M.W. Park, Thin Solid Films 517 (2009) 4196.
[12] D. Gong, C.A. Grimes, O.K. Varghese, W. Hu, R.S. Singh, Z. Chen, E.C. Dickey, J. Mater. Res. 16 (2001) 3331.
[13] K. Shankar, G.K. Mor, H.E. Prakasam, S. Yoriya, M. Paulose, O.K. Varghese, C.A. Grimes, Nanotechnology 18 (2007) 065707.
[14] V. Zwilling, M. Aucouturier, E. Darque-Ceretti, Electrochim. Acta 45 (1999) 921.
[15] V. Zwilling, E. Darque-Ceretti, A. Boutry-Forveille, D. David, M.Y. Perrin, M. Aucouturier, Surf. Interface Anal. 27 (1999) 629.
[16] P. Roy, D. Kim, I. Paramasivam, P. Schmuki, Electrochem. Commun. 11 (2009) 1001.
[17] M. Jin, X.T. Zhang, A.V. Emeline, T. Numata, T. Murakami, A. Fujishima, Surf. Coat. Technol. 202 (2008) 1364.
[18] L.X. Zhang, X.L. Wang, P. Liu, Z.X. Su, Surf. Coat. Technol. 201 (2007) 7607.
[19] X.Z. Liu, Y.H. Luo, H. Li, Y.Z. Fan, Z.X. Yu, Y. Lin, L.Q. Chen, Q.B. Meng, Chem. Commun. 27 (2007) 2847.
[20] R.J. Tayade, R.G. Kulkarni, R.V. Jasra, Ind. Eng. Chem. Res. 45 (2006) 922.
[21] J. Zheng, H. Yu, X. Li, S. Zhang, Appl. Surf. Sci. 254 (2008) 1630.
[22] D. Jiang, S. Zhang, H. Zhao, Environ. Sci. Technol. 41 (2007) 303.
[23] S. Ningshen, U. Kamachi Mudali, G. Amarendra, P. Gopalan, R.K. Dayal, H.S. Khatak, Corros. Sci. 48 (2006) 1106.
[24] B.C. O'Regan, S. Scully, A.C. Mayer, E. Palomares, J. Durrant, J. Phys. Chem. B 109 (2005) 4616.
[25] A. Zaban, M. Greenshtein, J. Bisquert, Chemphyschem 4 (2003) 859.
[26] P.M. Sommeling, B.C. O'Regan, R.R. Haswell, H.J.P. Smit, N.J. Bakker, J.J.T. Smits, J.M. Kroon, J.A.M. van Roosmalen, J. Phys. Chem. B 110 (2006) 19191.
[27] B.C. O'Regan, J.R. Durrant, P.M. Sommeling, N.J. Bakker, J. Phys. Chem. C 111 (2007) 14001.